Research Square

Preprints are preliminary reports that have not undergone peer review.
They should not be considered conclusive, used to inform clinical practice,
or referenced by the media as validated information.

Dose-Dependent Vibrational Response of Short-Chain DNA to Gamma Irradiation Modulated by Magnesium Ions

Kristina Serec
University of Zagreb
Maria Krajačić
maria.krajacic@mef.unizg.hr

University of Zagreb
Hrvoje Hršak
University of Zagreb
Ozren Gamulin
University of Zagreb
Sanja Dolanski Babić
University of Zagreb

Article

Keywords: Gamma irradiation, DNA-Mg2 + interactions, Co-60, FTIR spectroscopy, principal component analysis (PCA)

Posted Date: November 11th, 2026

DOI: https://doi.org/10.21203/rs.3.rs-11481237/v1

License: This work is licensed under a Creative Commons Attribution 4.0 International License.
Read Full License

Additional Declarations: No competing interests reported.

Dose-Dependent Vibrational Response of Short-Chain DNA to Gamma Irradiation Modulated by Magnesium Ions

Kristina Serec[a,b], Maria Krajačić[a]*, Hrvoje Hršak[a,c], Ozren Gamulin[a] and Sanja Dolanski Babić[a,b]
[a] Department of Physics and Biophysics, University of Zagreb School of Medicine, 10000 Zagreb, Croatia
[b] Centre of Excellence in Reproductive and Regenerative Medicine, University of Zagreb School of Medicine, 10000 Zagreb, Croatia
[c] University Hospital Centre Zagreb, 10000 Zagreb, Croatia
*To whom correspondence should be addressed. Email: maria.krajacic@mef.unizg.hr

Primary question: Does the FTIR fingerprint of short-chain DNA encode reproducible information about gamma-radiation exposure and absorbed dose?

Mechanistic question: How does the Mg^{2+} ion atmosphere modulate the spectral response of DNA to irradiation?

Proof-of-concept claim: Gamma irradiation produces reproducible dose-dependent vibrational perturbations in a controlled DNA–Mg^{2+} system, and the ionic environment changes how this response is expressed in multivariate spectral space.

Abstract

Rapid and reliable detection of ionizing radiation exposure is an emerging area of research, as accurate assessment of radiation-induced biological damage is important for protecting both patients and healthcare workers. Here, we developed a controlled DNA-Mg^{2+} model coupled with Fourier transform infrared (FTIR) spectroscopy to detect radiation-induced molecular changes and to establish a foundation for spectroscopic absorbed-dose assessment. We investigated a controlled short-chain double-stranded DNA-Mg^{2+} model at three Mg/P ratios, irradiated with Co-60 γ rays over an absorbed-dose range of 0.3-100 Gy using a clinical Gamma Knife unit. Irradiation-induced changes were detected across nucleobase, sugar-phosphate and conformation-sensitive spectral regions. Importantly, we found that the multivariate spectral response retains information related to absorbed dose, and that this dose-associated response is strongly modulated by the Mg^{2+} environment. Our findings indicate that the identified dose-sensitive spectral regions, and their Mg^{2+}-dependent modulation form a basis for spectroscopic absorbed-dose assessment. This provides a proof of concept for DNA-Mg^{2+}-based FTIR molecular radiation sensing and supports the need for further development of this approach as a rapid and reliable method for assessing radiation exposure and estimating absorbed dose.

Keywords: Gamma irradiation, DNA-Mg2+ interactions, Co-60, FTIR spectroscopy, principal component analysis (PCA)

1. Introduction

Ionizing radiation is widely used in medicine, from diagnostic imaging to high-energy therapeutic procedures. In this context, both patients and healthcare workers may be exposed to radiation fields that differ substantially in energy, dose rate and absorbed dose[1]. The biological response to ionizing radiation is strongly influenced by the physical characteristics of the radiation field, including radiation beam quality, linear energy transfer and absorbed dose[1,2]. Thus, understanding the biological effects of ionizing radiation in relation to its physical characteristics and absorbed dose is important for radiobiology and for the development of methods capable of detecting and characterizing radiation exposure.

Ionizing radiation induces structural and chemical changes at the molecular level, including interactions with DNA, which can subsequently lead to broader cellular and biological responses. For low-LET photon radiation, including γ rays, DNA damage may arise both from direct ionization of DNA and indirectly through reactive species generated predominantly by the radiolysis of water[2]. At the cellular level, the biological consequences of such damage depend strongly on subsequent DNA damage-response and repair processes[3]. Consequently, investigating radiation effects directly at the level of DNA in a controlled molecular environment provides a complementary approach to cellular radiobiology, allowing the initial molecular response to irradiation to be examined independently of downstream cellular processes.

At the molecular level, DNA represents one of the principal targets of ionizing radiation. Radiation-induced effects may involve modifications of nucleobases, perturbation of hydrogen bonding and base stacking, alterations of the sugar-phosphate backbone and, at higher levels of damage, single- and double-strand breaks[2,4,5]. Molecular modeling studies have further provided insight into ionization-induced bond dissociation and fragmentation pathways involving nucleobases and DNA[6]. Experimental studies using simplified DNA model systems have directly demonstrated radiation-induced strand damage under controlled conditions. Park et al. quantified single- and double-strand break formation in pBR322 plasmid DNA exposed to Co-60 γ rays and 1 MeV electrons, while Beaudier et al. used long-read sequencing to characterize dose-dependent fragmentation of dry pBR322 plasmid DNA following 3 MeV proton irradiation[7,8]. These studies illustrate the value of reduced DNA model systems for isolating radiation-induced molecular effects from the complexity of cellular and biological systems.

However, DNA does not respond to external perturbations as an isolated neutral molecule. Double-stranded DNA is a highly charged polyelectrolyte whose structural organization is governed by a balance between electrostatic interactions, hydrogen bonding, base stacking, hydration and counterion screening[9]. The negatively charged phosphate backbone is surrounded by an atmosphere of positive

counterions, which reduces electrostatic repulsion between phosphate groups and contributes to the stabilization of the double helix. Divalent cations such as Mg^{2+} are particularly important because of their efficient charge-compensating ability and their influence on the electrostatic and hydration environment of the DNA backbone[10-12].

The interaction of Mg^{2+} with DNA is predominantly governed by electrostatic screening of the negatively charged phosphate backbone and is closely related to the hydration state and local organization of the double helix[9,13] FTIR studies have shown that changes in the ionic atmosphere are reflected particularly in phosphate and sugar-phosphate vibrations and can be accompanied by changes in DNA conformational markers[14,15]. The balance between electrostatic screening, hydration and conformational stability becomes particularly important in short DNA fragments, where reduced chain length and dilute conditions limit collective polyion interactions[12,16]. Recent studies of ultra-short DNA further demonstrate that Mg^{2+} can stabilize the B-form under such conditions, confirming the important role of the ionic environment in determining DNA conformation[17,18]. These observations indicate that the counterion environment can alter the structural background against which externally induced perturbations of DNA are expressed.

This aspect may be particularly relevant for radiation-induced changes. The molecular environment surrounding DNA can substantially influence its response to ionizing radiation. For example, ectoine has been shown to reduce radiation-induced single- and double-strand breaks in plasmid DNA, demonstrating that changes in the local physicochemical environment can modify radiation damage[19]. Mg^{2+} has likewise been proposed to stabilize DNA structure and to reduce damage associated with free-radical processes, suggesting a possible protective role under irradiation conditions[20]. Nevertheless, the extent to which the Mg^{2+} ion atmosphere modulates the vibrational response of DNA to ionizing radiation remains insufficiently characterized. In particular, it is not clear whether changes in Mg^{2+}-mediated charge screening merely alter the magnitude of the radiation response or whether they modify how that response is expressed across nucleobase, phosphate, sugar-phosphate and conformation-sensitive vibrations.

Fourier transform infrared spectroscopy provides a suitable approach for addressing this question because it probes the molecular fingerprint of DNA and can detect coordinated changes distributed over multiple spectral regions. Previous infrared and Raman studies have demonstrated sensitivity to radiation-induced biochemical changes in isolated DNA, cells, blood and tissues[21–29]. More recent studies have extended this approach to low-dose exposure and contemporary radiotherapy conditions. Inman et al. demonstrated FTIR-detectable molecular signatures following low-dose X-ray exposure in vivo and showed that FTIR could discriminate radiation exposure down to the sub-Gy range[30]. Infrared microspectroscopy has also been used to investigate molecular responses under FLASH radiotherapy conditions, revealing contributions from proteins, lipids and nucleic-acid-associated spectral regions[31]. Thus, much of the spectroscopic work on radiation response has been performed in complex biological systems, where the measured infrared fingerprint reflects overlapping contributions from proteins, lipids, carbohydrates and nucleic acids[30,31].

Although such studies are highly relevant for biological dosimetry, they make it difficult to isolate the direct molecular response of DNA itself. Recent studies of radiation effects in simplified DNA model systems have therefore emphasized the importance of reducing biological complexity in order to resolve DNA-specific effects. For example, Wanstall et al. used plasmid DNA as a controlled model to investigate radiation-induced strand damage independently of DNA repair and other cellular pathways[32]. However, direct vibrational characterization of isolated DNA under controlled ionic conditions remains scarce. In particular, it is not known how the counterion environment modulates the spectroscopic response of DNA to γ irradiation or whether this response retains systematic information related to absorbed dose.

For controlled irradiation of DNA, Co-60 γ radiation provides a clinically relevant high-energy photon source with well-defined irradiation conditions. The Gamma Knife unit, in which multiple Co-60 beams converge on a defined target volume, is particularly suitable for controlled irradiation experiments because its irradiation geometry enables highly accurate and reproducible dose delivery[33]. The overall

spatial accuracy of Gamma Knife irradiation is generally within the submillimetre range under controlled conditions, although it may be affected by uncertainties associated with image localization, image registration, and target positioning. Computed tomography imaging can be used in combination with Gamma Knife treatment planning to define the stereotactic geometry and accurately position the target relative to the irradiation isocenter. Thus, a clinically established Gamma Knife unit provides a well-defined platform for investigating dose-dependent molecular responses under controlled conditions.

In the present study, we investigated whether the vibrational fingerprint of ultra-short double-stranded DNA can be used to detect and characterize molecular changes induced by γ irradiation and how these changes are modulated by the surrounding Mg^{2+} ion atmosphere. DNA samples were investigated under three magnesium-to-phosphate conditions, defined by r = [Mg]/[P] = 1, 0.1 and 0.01 and irradiated with Co-60 γ rays over an absorbed-dose range of 0.3-100 Gy. By combining FTIR spectroscopy with irradiation–control difference spectra and principal component analysis, we show that irradiation-induced changes can be detected across nucleobase, sugar–phosphate and conformation-sensitive spectral regions, even for the lowest investigated dose of 0.3 Gy. Importantly, the spectral response is strongly modulated by the Mg^{2+} ion atmosphere, demonstrating that the ionic environment influences how radiation-induced perturbations are expressed within the DNA vibrational fingerprint. The resulting multivariate organization further retains systematic information related to absorbed dose. Together, these findings provide a proof-of-concept basis for FTIR-based molecular radiation sensing and establish a framework that could be further developed toward the detection and quantitative estimation of absorbed dose.

2. Materials and Methods

In this study, we investigated the influence of Co-60 gamma irradiation on short-chain DNA samples prepared under different Mg^{2+} ionic conditions and irradiated at doses ranging from 0.3 to 100 Gy. The experimental protocol consisted of four main steps: preparation of DNA solutions, irradiation of the DNA solutions, preparation of DNA thin films from the irradiated solutions, and acquisition of FTIR spectra from the resulting thin films.

2.1 DNA solution preparation

DNA solutions were prepared from short-chain herring Na-DNA fragments, 15–50 bp in length, obtained from Sigma-Aldrich and used without further purification. $MgCl_2$, purchased from Sigma-Aldrich, was dissolved in ultrapure Milli-Q water and used to prepare DNA solutions with a final DNA concentration of 1 g/L, corresponding to a DNA phosphate concentration of 3 mM.

To investigate the influence of the Mg^{2+} ionic environment, DNA samples were prepared at three distinct magnesium-to-phosphate molar concentration ratios defined as r = [Mg]/[P] = 1, 0.1 and 0.01. Our previous work showed that weak ionic screening is associated with reduced conformational stability of ultra-short DNA, whereas increasing r enhances phosphate charge screening and stabilizes the B-form. Based on these findings, the selected Mg/P ratios were chosen to span a broad range of Mg^{2+}-mediated electrostatic screening[14,18]. According to our previously established protocol for strict control of the DNA ionic atmosphere, no additional buffers were used, and the solutions were allowed to equilibrate for 48 h to ensure sample homogeneity[15].

2.2 Gamma irradiation of DNA solutions

DNA solutions were irradiated using Co-60 gamma rays delivered by Leksell Gamma Knife Icon unit (Elekta Instrument AB, Stockholm, Sweden) and routinely used for stereotactic brain radiosurgery at the University Hospital Centre Zagreb.

For irradiation, the DNA solutions were placed in a custom-made 3D-printed spherical insert positioned within a spherical (d = 16 cm) polymethyl methacrylate (PMMA) phantom and aligned with the irradiation

isocentre of the Gamma Knife unit (Fig. 1). The insert was fabricated from tissue-equivalent plastic to ensure reproducible sample positioning during irradiation.

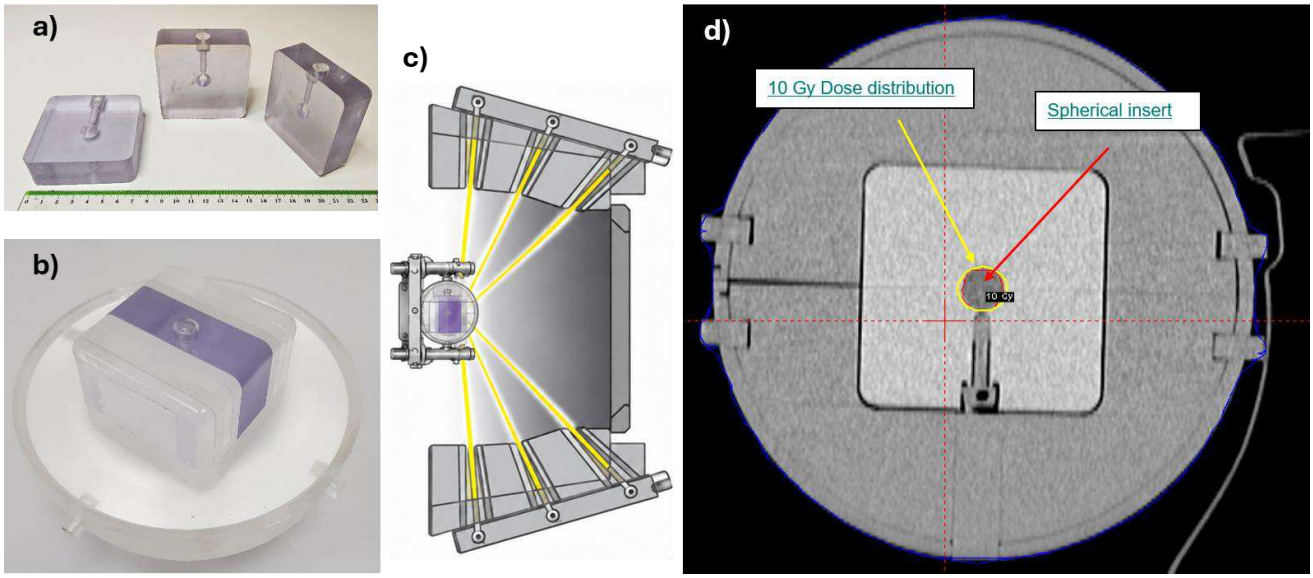


Figure 1.

Non-irradiated samples served as controls (0 Gy), while the irradiated samples received absorbed doses of 0.3, 1, 10, 30, or 100 Gy at a dose rate of 1.565 Gy/min. The experimental design therefore comprised 18 different sample conditions: five irradiation doses (0.3, 1, 10, 30, and 100 Gy) and three magnesium ion environments (r = 1, 0.1 and 0.01). Table 1 presents the delivered absorbed doses with associated uncertainties. Absorbed dose calculation was carried out over the solution sample volume, divided into 1 mm^3 calculation voxels.

Prior to irradiation, the phantom with an empty insert was imaged using the CT unit SOMATOM Definition As+ (Siemens, Erlangen, Germany). CT images were imported into the treatment planning software Leksell GammaPlan (Elekta Instrument AB, Stockholm, Sweden) and used to define the irradiation geometry, align the phantom to the Gamma Knife unit isocenter and calculate absorbed dose (Fig. 1d). The dose rate at the isocenter of the Gamma Knife unit was verified using a thimble ionization chamber Semiflex TM31010 (PTW, Freiburg, Germany) in conjunction with the electrometer UNIDOS E (PTW, Freiburg, Germany). After the absorbed dose calculation, the insert was filled with the DNA solution sample, adjusted to the Gamma Knife unit isocenter, and irradiated.

Table 1.

DNA solution sample (Volume = 1 mL)	Dose delivered to the sample (Gy)	Irradiation time (min)
Control	0.0 ± 0.0	0.00
Dose 1	0.3 ± 0.0	0.20
Dose 2	1.0 ± 0.0	0.65
Dose 3	10.0 ± 0.1	6.51
Dose 4	30.0 ± 0.4	19.53
Dose 5	100.0 ± 1.4	65.10

2.3 DNA thin-film preparation and FTIR spectral acquisition

Following irradiation, DNA thin films were prepared from the irradiated DNA solutions. Highly hydrated DNA thin films provide a biologically relevant system suitable for FTIR spectroscopy while avoiding the strong contribution of bulk water and thus the associated need for water subtraction.

For thin-film preparation, 30 µL of each DNA solution was deposited onto optical-grade silicon transmission windows and dried in a desiccator for 10 min using a rotary vacuum pump, with a final pressure of approximately 10 mbar. This procedure removes excess bulk water while retaining a highly hydrated DNA film, thereby reducing the strong infrared contribution of liquid water while preserving a hydrated molecular environment around the DNA. Although such thin films do not fully reproduce the aqueous environment of DNA in solution, they provide a controlled and well-characterized model for FTIR analysis. In our previous studies, the effects of drying time and hydration level on DNA vibrational signatures were systematically investigated, allowing hydration-driven spectral changes to be distinguished from ion-mediated structural effects. Importantly, all samples in the present study were prepared and measured under identical hydration and drying conditions, enabling direct comparison of irradiation-induced spectral changes across Mg^{2+} conditions and absorbed doses[15,34]. The estimated relative humidity of the resulting thin films was approximately 85 %, consistent with our previously established preparation protocol[14].

FTIR spectra were recorded using a PerkinElmer Spectrum GX spectrometer equipped with a liquid-nitrogen-cooled mercury cadmium telluride (MCT) detector and a KBr beam splitter. Spectra were acquired in transmission mode at 25 °C with a spectral resolution of 4 cm^{-1} and 32 co-added scans per spectrum. Approximately 10 replicate thin films were prepared and measured for each of the 18 experimental conditions.

2.4 Spectral preprocessing and principal component analysis

Spectral preprocessing, descriptive spectral analysis, and chemometric analysis were performed using custom Python scripts developed in a Jupyter Notebook environment (Python 3.13.9). Additional analyses were performed using MATLAB 2010 (MathWorks, Natick, MA, USA) and OriginPro 2019 (OriginLab Corp., Northampton, MA, USA).

For calculation of the average and difference spectra, raw FTIR spectra were baseline-corrected and normalized according to our previously established protocol[15]. An average spectrum was calculated for each of the 18 experimental conditions from the corresponding replicate spectra (≈ 10 replica). Radiation-induced difference spectra were subsequently calculated for each magnesium concentration by subtracting the average spectrum of the corresponding non-irradiated control from the average spectrum obtained at each irradiation dose (Dose - Control).

Principal component analysis (PCA) was used to identify systematic spectral variations associated with irradiation dose at each magnesium-to-phosphate ratio. PCA reduces the dimensionality of spectral datasets by transforming the original correlated spectral variables into a smaller number of orthogonal principal components (PCs). The resulting PC scores describe the distribution of the samples in the reduced-dimensional space, whereas the corresponding loading vectors identify the spectral variables contributing most strongly to each principal component.

Several spectral preprocessing approaches were evaluated prior to PCA. The preprocessing procedure used for the presented PCA models consisted of adaptive iteratively reweighted penalized least-squares (airPLS) baseline correction, standard normal variate (SNV) transformation, and generalized least-squares weighting (GLSW)[35–37]. PCA was then performed using the preprocessed spectra, and the first six principal components were retained for analysis. PC scores were used to evaluate dose-dependent sample distributions, whereas PC loadings were examined to identify the spectral regions contributing to the observed separation. All figures presented were generated using Python (3.13.9) in a Jupyter Notebook environment.

3. Results

3.1 Overall FTIR characteristics of non-irradiated DNA

The non-irradiated short-chain DNA thin films exhibited the characteristic vibrational fingerprint of DNA between 1800 and 700 cm⁻¹. The corresponding control spectra (0 Gy) for *r* = 1, 0.1 and 0.01 are shown in black in Fig. 2a–c, respectively. The DNA fingerprint region can be divided into three spectral regions according to the molecular groups contributing predominantly to the observed vibrations. The respective spectral regions, together with the principal vibrational bands and their literature-based tentative assignments, are described in the following paragraphs and summarized in Table 2.

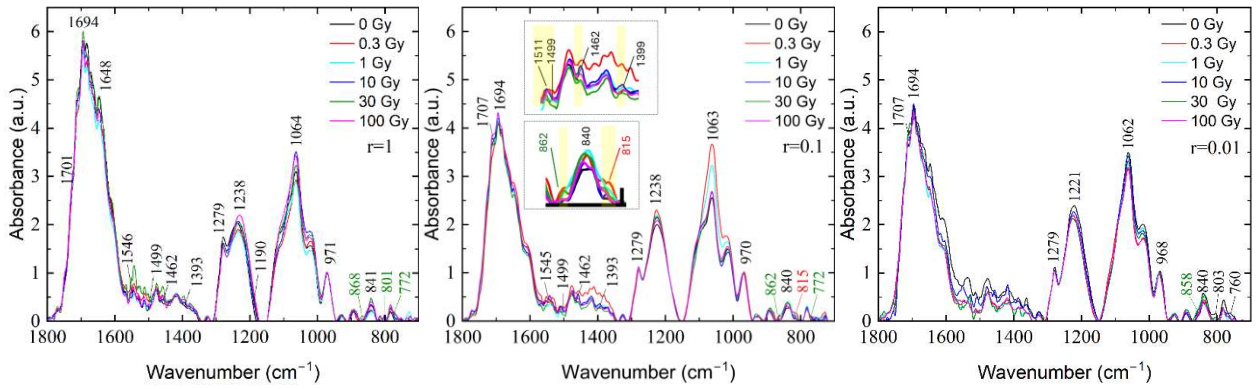


Figure 2.

Table 2.

Band position (cm⁻¹)	Tentative assignment
1701	C=O stretching vibration
1694	C=O stretching vibration
1648	C=O/C=C/C=N contributions
1546	C=N and C=C contributions
1471	C=N-associated base vibration
1238	Asymmetric PO_2^- stretching vibration
1190	C3′-endo-associated sugar–phosphate vibration
1089	Symmetric PO_2^- stretching vibration
1064	C–O phosphodiester vibration
971	Deoxyribose C–C vibration
893	Deoxyribose/backbone vibration
868	C3′-endo-associated vibration; A-form marker
841	C2′-endo-associated vibration; B-form marker
801	C3′-endo-associated vibration; A-form marker

The analysis begins with the 1800–1300 cm⁻¹ region, dominated by vibrations of the nucleobases adenine, thymine, cytosine and guanine, including modes involving C=O, C=N, C=C and C-N bonds, together with other coupled base vibrations. Among the assigned features, bands near 1701 and 1694 cm⁻¹ are located in the carbonyl-dominated region and are predominantly associated with nucleobase C=O stretching vibrations. A feature near 1648 cm⁻¹ is assigned more broadly to overlapping base-associated stretching modes, including contributions from C=O, C=C and C=N vibrations, while the band near 1546 cm⁻¹ is attributed to coupled nucleobase ring vibrations with possible C=N and C=C contributions. In addition to these assigned bands, Figs. 2 and 3 also highlight several weaker spectral

features and shoulders that were selected because they exhibited reproducible changes following irradiation. These features do not necessarily correspond to the most intense absorption maxima in the non-irradiated spectra, and some cannot be uniquely assigned because of extensive overlap between nucleobase vibrational modes. Table 2 therefore summarizes the principal bands for which sufficiently supported literature-based assignments could be made.

Moving towards lower wavenumbers, the 1300-900 cm^{-1} region is predominantly associated with the sugar-phosphate backbone. Characteristic bands include the asymmetric PO_2^- stretching vibration near 1232 cm^{-1}, the C3′-endo-associated sugar-phosphate vibration near 1185 cm^{-1}, the symmetric PO_2^- stretching vibration near 1089 cm^{-1}, and C-O phosphodiester and deoxyribose-related vibrations at lower wavenumbers. These bands provide information on the local environment and organization of the DNA sugar–phosphate backbone.

The spectral region below 900 cm^{-1} contains several vibrations particularly sensitive to DNA backbone conformation and deoxyribose puckering. Bands at approximately 868, 841 and 801 cm^{-1} have been associated with C3′-endo- and C2′-endo-related sugar conformations and are therefore commonly used as markers of DNA conformational state[14,17,18].

Additionally, comparison of the non-irradiated spectra (0 Gy) shown in Fig. 2 revealed [Mg]/[P]-dependent differences in band position, relative intensity and spectral profile across the investigated fingerprint region. A detailed analysis of these Mg^{2+}-dependent differences is beyond the scope of the present study. Here, the non-irradiated spectra are used solely as a reference (control group) for evaluating irradiation-induced spectral changes in the corresponding Mg/P conditions.

3.2 Gamma irradiation induces dose-dependent changes in the average FTIR spectra

Following *γ* irradiation, the overall FTIR fingerprint of short-chain DNA remained preserved throughout the investigated dose range (Fig. 2). Irradiation-associated spectral changes were nonetheless detectable even at the lowest investigated absorbed dose of 0.3 Gy and became more pronounced or underwent further restructuring with increasing dose. The dose-dependent response involved changes in band intensity, position and profile across the nucleobase, sugar-phosphate backbone and conformation-sensitive regions.

For the highest magnesium-to-phosphate ratio (r = 1), where the irradiation-induced changes were most clearly resolved in the average spectra, modifications were apparent already at 0.3 Gy (Fig. 2a). In the nucleobase region, changes were observed around the carbonyl-dominated bands near 1701 and 1694 cm^{-1} and in additional features near 1648, 1546, 1499, 1462 and 1393 cm^{-1}. Several of these modifications became increasingly apparent at higher doses. In particular, the initially weak feature near 1499 cm^{-1} increased in intensity and shifted toward higher wavenumbers, while the regions near 1462 and 1393 cm^{-1} showed progressive restructuring, with the largest modifications generally observed at 30 and 100 Gy.

Dose-dependent changes were also evident in the sugar-phosphate backbone region. The asymmetric phosphate stretching region near 1230 cm^{-1} underwent progressive restructuring, accompanied by changes in the neighboring region around 1190 cm^{-1}. Modifications were additionally observed around the symmetric phosphate vibration near 1090 cm^{-1} and within the C-O/phosphodiester and deoxyribose-associated bands at lower wavenumbers. Several of these backbone-related changes were detectable at 0.3 Gy and increased in magnitude or complexity with increasing absorbed dose.

In the conformation-sensitive region below 900 cm^{-1}, irradiation-associated changes were also evident at r = 1. These included broadening of the band near 893 cm^{-1}, increased prominence of features near 868,

816-814, and 801 cm^{-1}, and the appearance of a more distinct shoulder near 772 cm^{-1} at higher absorbed doses.

At lower Mg/P ratios (Fig. 2b and 2c), irradiation-associated changes remained evident across the same major spectral regions. For r = 0.1 (Fig. 2b), pronounced modifications were observed in the nucleobase region, particularly around 1707-1694, 1499 and 1462-1393 cm^{-1}. The most pronounced changes were observed in the 1511-1499 cm^{-1} region, where the band at 1511 cm^{-1} became more pronounced with increasing absorbed dose. In addition, a distinct response was observed near 1462 cm^{-1}, where an initial shoulder developed into a clearly resolved spectral feature, while smaller modifications were also evident near 1399 cm^{-1}. Changes were additionally observed in the sugar–phosphate backbone, particularly near 1238 and 1063 cm^{-1}, and in the conformation-sensitive region around 862, 840, and 815 cm^{-1}.

At r = 0.01 (Fig. 2c), irradiation-associated modifications remained observable across the DNA fingerprint, although individual spectral changes were less distinctly resolved in the average spectra. Changes were nevertheless evident in the nucleobase, sugar-phosphate, and conformation-sensitive regions, indicating that the irradiation response persisted under the lowest Mg^{2+} condition but was expressed as a broader and less clearly resolved redistribution of spectral intensity.

3.3 Difference spectra enhance low-dose irradiation-induced spectral changes

To further resolve irradiation-induced spectral changes, difference spectra were calculated for each Mg/P ratio as $\Delta A = A_{dose} - A_{control}$, where ΔA is the difference absorbance spectrum, A_{dose} is the absorbance spectrum at a given irradiation dose, and $A_{control}$ is the corresponding non-irradiated spectrum for the same Mg/P ratio. The resulting difference spectra are presented in Fig. 3. Importantly, irradiation-associated difference features were already detectable at the lowest investigated absorbed dose of 0.3 Gy, confirming the sensitivity of the FTIR fingerprint to low-dose γ irradiation. The difference spectra obtained for r = 1 (Fig. 3a) revealed that the most prominent irradiation-induced changes were observed in the sugar-phosphate backbone region. A broad and intense difference feature centred at approximately 1196 cm^{-1} was already evident at 0.3 Gy and became progressively more pronounced with increasing dose. A strong dose-dependent response was also observed in the region of the symmetric phosphate stretching vibration, reflected by progressively increasing difference features near approximately 1086 and 1097 cm^{-1}. Additional changes were evident around 1057 and 1000 cm^{-1}, corresponding to neighbouring phosphodiester- and deoxyribose-associated vibrations. In the nucleobase region, clear and pronounced difference features were already observed at the lowest investigated dose of 0.3 Gy, particularly near 1682 and 1457 cm^{-1}. Additional irradiation-associated features were observed near 1548, 1487 and 1398 cm^{-1}, with their magnitude generally increasing or undergoing further restructuring at higher absorbed doses. Finally, irradiation-associated difference features were clearly observed in the conformation-sensitive region, with distinct peaks near 867, 841, 823, 813 and 782 cm^{-1}.

At r = 0.1 (Fig. 3b), the difference spectra similarly confirmed irradiation-induced changes in the nucleobase region, while marked changes were also observed within the sugar-phosphate backbone, particularly near the asymmetric phosphate stretching region around 1228 cm^{-1} and near 1067 cm^{-1}. The conformation-sensitive region showed distinct features near 856, 838 and 802 cm^{-1}.

At the lowest Mg/P ratio, r = 0.01 (Fig. 3c) irradiation-associated difference features remained detectable across the nucleobase and sugar–phosphate regions. Interestingly, the conformation-sensitive region became more clearly resolved in the difference spectra, with pronounced features near 863, 828 and 806 cm^{-1}.

Overall, the difference spectra demonstrate that FTIR detects γ irradiation-induced molecular changes already at 0.3 Gy, while the magnitude and spectral distribution of these changes continue to evolve across the investigated dose range. The response is not uniform across molecular regions or Mg/P conditions, indicating that different parts of the DNA vibrational fingerprint contribute differently to the dose-dependent spectral response.

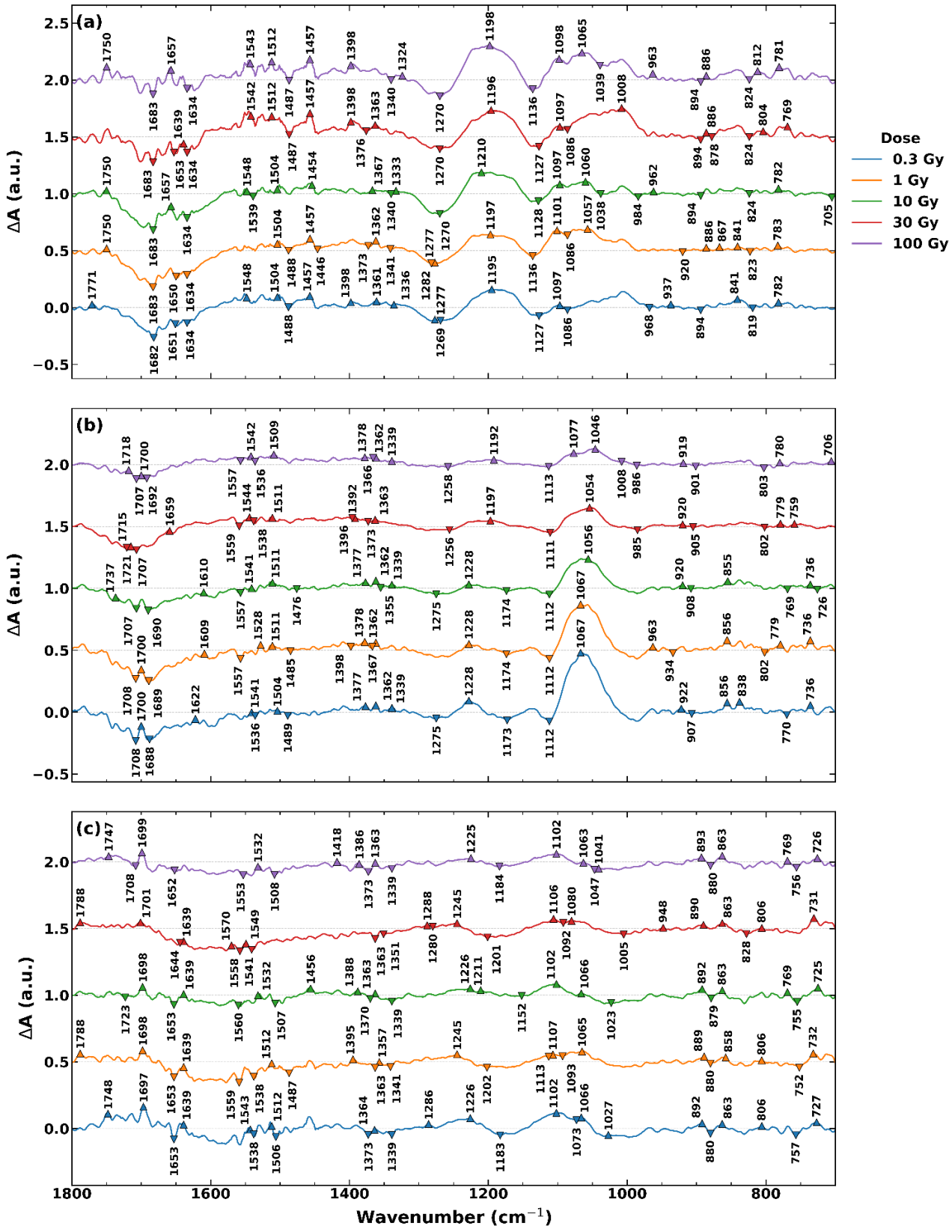


Figure 3.

3.4 Principal component analysis of irradiation-induced spectral variation

Principal component analysis was performed separately for each of the Mg/P ratio, r = 1, 0.1 and 0.01, with the corresponding score plots shown in Figs. 4a-c, respectively. For all three Mg/P conditions, the non-irradiated controls occupied a distinct region of the PCA score space relative to the irradiated samples, indicating systematic irradiation-associated differences in the FTIR fingerprint.

At r = 1 (Fig. 4a), PC1 accounted for 59.86 % of the variance and provided the dominant separation between non-irradiated and irradiated samples. The 0 Gy controls exhibited negative PC1 scores, whereas irradiated samples were shifted toward more positive values. Within the irradiated group, the lower doses (0.3-10 Gy) remained relatively close to one another, followed by a pronounced additional positive displacement at 30 and 100 Gy. At r = 0.1 (Fig. 4b), the irradiation-associated separation was primarily expressed along PC2 (23.61 %), with additional organization along PC3. The 0.3 and 1 Gy groups showed an overlap, whereas the 10, 30, and 100 Gy samples occupied more distinct regions of the PC2-PC3 score space. At r = 0.01 (Fig. 4c), the main irradiation-associated variation was represented by PC3 (9.16 %), while PC4 further contributed to the clustering of irradiated samples. Overall, irradiation-associated separation was primarily represented by PC1 at r = 1, PC2 at r = 0.1, and PC3 at r = 0.01, while separation between non-irradiated and irradiated spectra remained evident under all three ionic conditions.

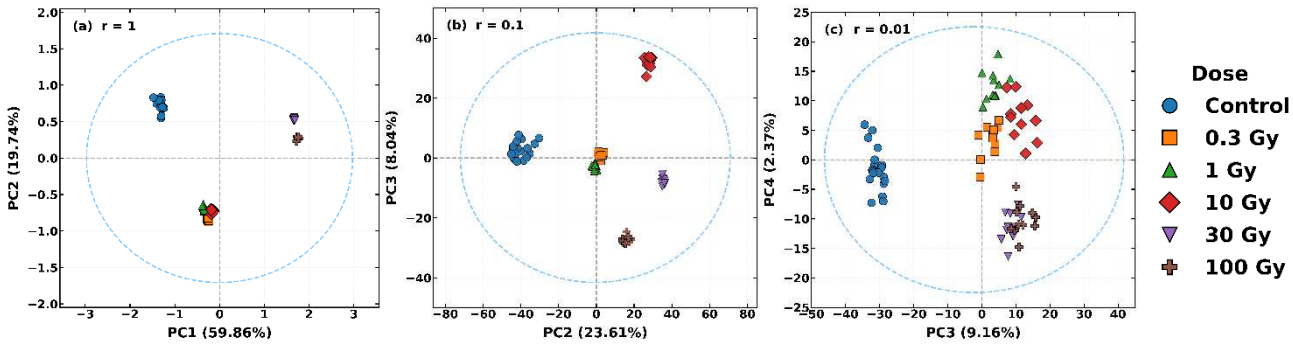


Figure 4.

To further investigate the spectral features contributing to the observed sample separation, the corresponding PCA loadings were examined. The resulting loading profiles, presented in Figure 5, provide insight into the spectral regions associated with the observed clustering pattern (Fig. 4). Specifically, Figure 5a presents the loading profile for the highest Mg/P ratio (r = 1), whereas Figure 5b corresponds to the lowest Mg/P ratio (r = 0.01). The loading sign was interpreted together with the corresponding score distribution. Namely, the PC score is calculated as a weighted linear combination of the original spectral variables. Thus, variables with positive loadings contribute to more positive scores as their values increase, whereas variables with negative loadings contribute to more negative scores[40]. Consequently, the loading sign indicates whether a spectral variable contributes to the positive or negative direction of the corresponding PC score.

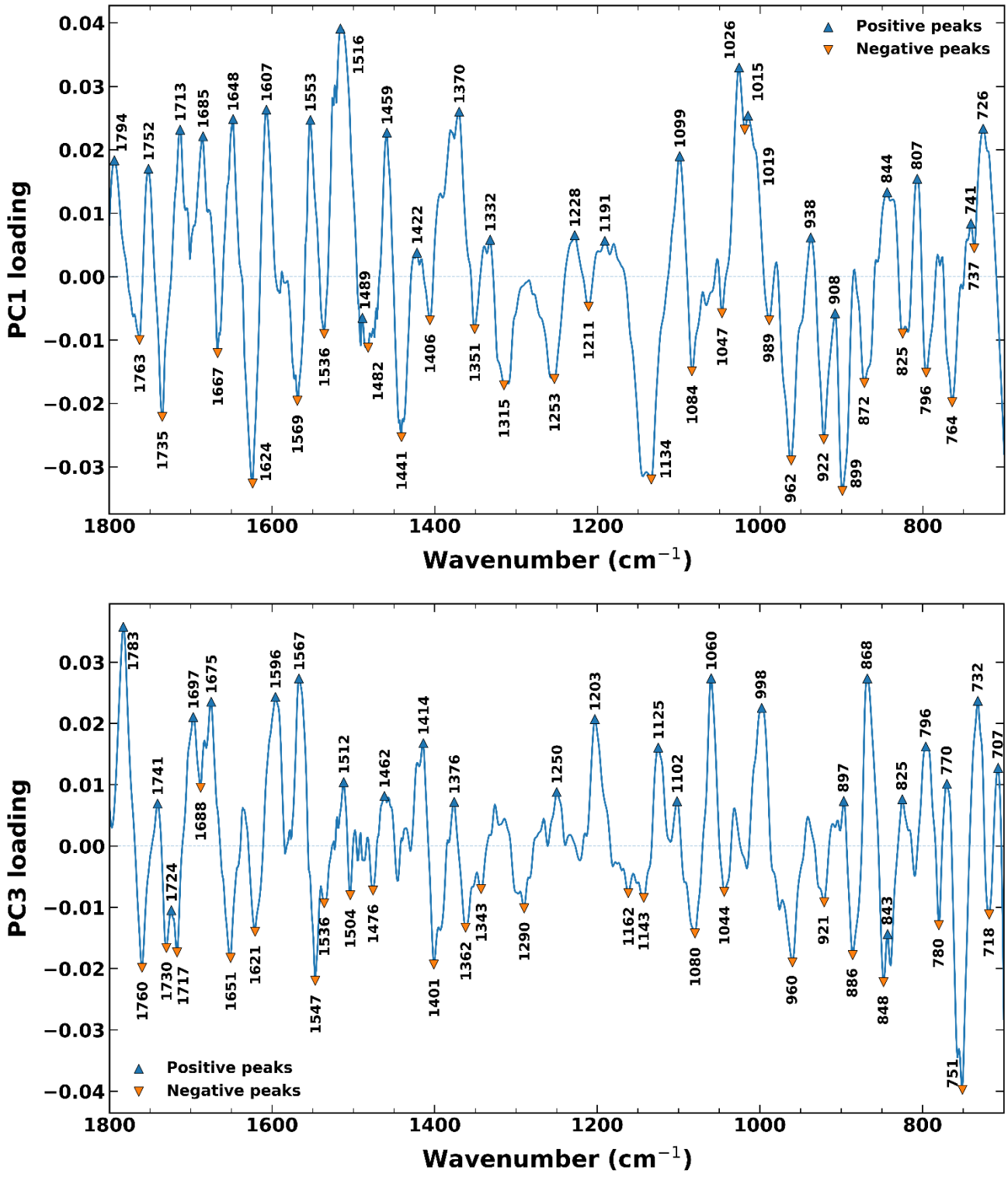


Figure 5.

As shown in Fig. 4, the control group occupies the negative score direction for all Mg^{2+} concentrations, whereas the irradiated samples are shifted toward more positive scores. Accordingly, positive loading features are associated with samples positioned toward the positive PC scores, corresponding to the irradiated group of samples, whereas negative loadings are associated with the samples positioned toward negative PC scores, corresponding to the control group.

Focusing first on the loading profile obtained for $r = 1$ (Fig. 5a), several spectral features contributing to the observed separation can be identified. A closer examination of the nucleobase region reveals prominent loading features near 1713, 1685, 1648, 1607, 1553, 1516, 1459 and 1370 cm^{-1}. Several of these coincide with, or lie close to, irradiation-responsive features observed independently in the average and difference spectra (Figs. 2 and 3). Specifically, the peak at 1516 cm^{-1} represents the strongest positive loading contribution in the entire PC1 profile. Within the sugar-phosphate region, strong positive loading features are observed near 1099 and 1026 cm^{-1}. In comparison, the positive contribution near 1228 cm^{-1}, corresponding to the asymmetric PO_2^- stretching region, is considerably smaller. In the conformation-sensitive region below 900 cm^{-1}, pronounced loading features are observed near 872, 844, 825 and 807 cm^{-1}. The bands at 844 and 807 cm^{-1} contribute positively to the PC1 and are therefore associated with the irradiation-related direction, whereas bands near 872 and 825 cm^{-1} have negative contributions and are associated with the control direction.

The analysis of the PC3 loading profile for the lowest Mg/P ratio ($r = 0.01$) given in Fig. 5b, shows prominent positive features in several spectral regions. As shown by the corresponding score plot (Fig. 4c), the control group is located on the negative PC3 axis, whereas the irradiated samples are shifted toward more positive PC3 scores; thus, positive loading features are associated with the irradiation-related direction of the PCA space. In the nucleobase region, prominent positive features occur near 1699, 1675 and 1567 cm^{-1}. A positive contribution is also present near 1512 cm^{-1}. Interestingly, it is considerably less pronounced than the corresponding ~1516 cm^{-1} feature at $r = 1$, which represents the dominant positive loading in the PC1 profile. A particularly distinct pattern is observed in the conformation-sensitive region below 900 cm^{-1}. The band near 868 cm^{-1} is one of the most prominent loading features in the whole PC3 profile showing the strongest positive contribution within the conformation-sensitive region. This positive contribution associates the band with the irradiation-related direction of the PC3 space, in agreement with the corresponding score distribution from Fig. 4c. Another positive loading peak is also observed near 825 cm^{-1}, whereas neighboring features near 848–843 cm^{-1} are associated with the negative, control-related direction.

3.5 Dose-dependent principal-component score trajectories

To further explore the relationship between irradiation dose and the obtained PCA scores, the corresponding PC scores were analysed as a function of absorbed dose. For each Mg/P ratio, the principal component showing the clearest separation between the control and irradiated samples was identified. The scores of individual spectra were then plotted according to the corresponding dose group, together with the mean score values and associated error bars to provide a more direct representation of the dose-associated changes. Figure 6 presents the obtained PC scores together with the mean PC1, PC2, and PC3 scores for $r = 1$, $r = 0.1$ and $r = 0.01$ respectively. Additionally, the corresponding standard deviations for each absorbed dose are also presented as error bars. This representation allows the progression of the mean PCA score to be followed directly across the investigated absorbed-dose range for each Mg/P condition.

At the highest Mg/P ratio, $r = 1$ (Fig. 6a), the non-irradiated samples exhibited strongly negative PC1 scores, while all irradiated samples were shifted toward higher (more positive) values. The mean PC1 scores for absorbed doses of 0.3, 1, and 10 Gy remained relatively close, whereas a pronounced increase was observed at 30 and 100 Gy.

At the intermediate Mg/P ratio, $r = 0.1$ (Fig. 6b), PC2 scores showed a marked shift from the non-irradiated controls to the irradiated samples. However, the dose-dependent trajectory differed from that observed at $r = 1$. However, a somewhat different pattern was observed. The mean PC2 scores increased from 0.3 Gy to 30 Gy, reaching the highest values at 30 Gy. A further increase of the absorbed dose to 100 Gy resulted in a decrease in the mean PC2 score. Despite the decrease, the value remained positive, indicating a clear separation from the control group.

Finally, at r = 0.01 (Fig. 6c), PC3 scores shifted markedly from negative values in the non-irradiated controls toward positive values after irradiation. Although some adjacent dose groups partially overlapped, the mean PC3 score showed an overall increase across the investigated dose range.

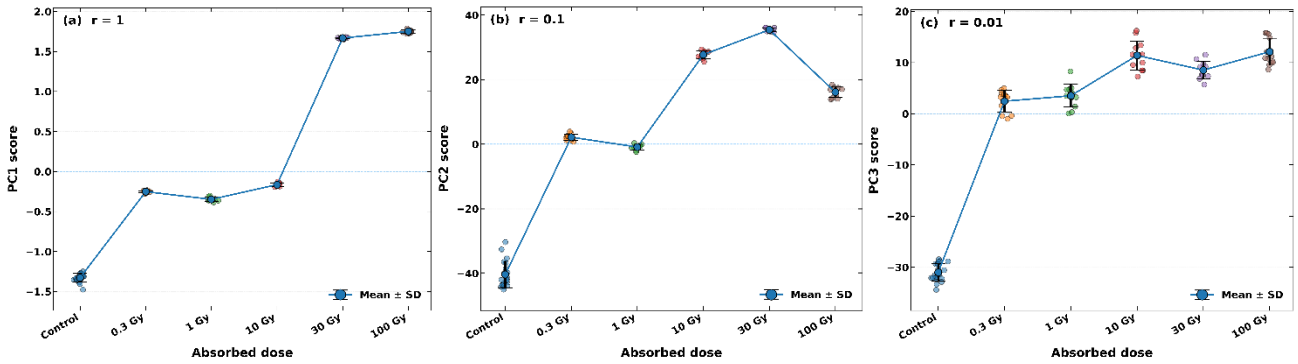


Figure 6.

Overall, the shape of the dose-dependent score response differed markedly with Mg/P ratio. At r = 1, a pronounced increase in PC1 score was observed at 30 and 100 Gy. At r = 0.1 the mean PC2 score began to increase at lower absorbed doses, with a clear increase evident at 10 Gy, while for r = 0.01, a shift in the mean PC3 score was observed even for the lowest investigated dose of 0.3 Gy. Thus, the distribution of PCA scores and their respective grouping across absorbed doses depended strongly on the Mg^{2+} environment.

4. Discussion

The discussion is organized around three main findings of this study. First, we examine whether the FTIR fingerprint of short-chain DNA provides a detectable molecular signature of γ radiation exposure, with particular emphasis on changes observed at the lowest investigated dose of 0.3 Gy. Second, we consider how the Mg^{2+} ion atmosphere modifies the molecular and conformational response of DNA to irradiation. Finally, we evaluate whether the systematic dose-associated organization observed in multivariate spectral space supports the use of the DNA-Mg^{2+} system as a proof-of-concept platform for molecular radiation sensing.

A key outcome of the present study is the establishment of a controlled short-chain DNA-Mg^{2+} model in which irradiation-associated molecular changes can be detected by FTIR spectroscopy. Our results clearly demonstrate that the response of short-chain DNA to γ irradiation involves nucleobase-associated vibrations, phosphate and phosphodiester groups, deoxyribose-related modes and conformation-sensitive bands, indicating that irradiation affects multiple regions of the DNA vibrational fingerprint. These irradiation-associated spectral modifications were detectable at the lowest investigated absorbed dose of 0.3 Gy and were consistently observed within defined spectral regions.

The sensitivity of vibrational spectroscopy to radiation-induced molecular changes has been demonstrated across various biological systems and irradiation modalities. Inman et al. recently showed that FTIR-ATR spectroscopy combined with computational analysis could detect X-ray exposure in vivo down to 0.1 Gy[30], with discriminative spectral features associated in part with DNA conformational changes. Although their study was performed in a complex biological tissue, in contrast to the controlled DNA-Mg^{2+} system used in the present study, both studies demonstrate that low-dose ionizing radiation can produce vibrational signatures detectable by FTIR spectroscopy.

Previous vibrational spectroscopic studies have established that phosphate, phosphodiester and sugar-related vibrations can respond to ionizing radiation, particularly in cells and tissues. However, many of

these studies were performed at substantially higher absorbed doses than those investigated here[22,25,41,42]. In the present study, however, these backbone-associated changes are demonstrated even at the lowest absorbed doses (0.3 Gy) and in a chemically controlled short-chain DNA-Mg^{2+} system. Moreover, the response is not limited to a single spectral feature, but is expressed coherently across phosphate stretching, phosphodiester, deoxyribose and conformation-sensitive regions and is further modulated by the Mg^{2+}/P ratio. In our work, particularly pronounced irradiation-associated changes were observed near 1196 cm^{-1} band, in the region between 1086 and 1097 cm^{-1}, as well as around 1057 and 1000 cm^{-1}. All of these bands are associated with the phosphodiester/deoxyribose backbone. Additionally, changes are also evident in the conformation-sensitive region near 867, 841, 823, 813 and 782 cm^{-1}. These findings, therefore, suggest that the sugar–phosphate backbone is a major contributor to the FTIR-detectable response of short-chain DNA to γ irradiation.

In the present study, we further demonstrate that irradiation-associated changes are also clearly expressed in the nucleobase region. In the carbonyl-dominated section around 1700 cm^{-1}, where nucleobase C=O stretching vibrations make a major contribution to the spectral profile, irradiation-associated modifications were observed near 1701-1694 cm^{-1}. These changes are particularly evident in the difference spectra shown in Fig. 3a, as well as in the corresponding PCA loading profile, providing consistent evidence that this region contributes to the irradiation-induced spectral response. Since there are several carbonyl-containing bases contributing to this region and the corresponding vibrations overlap strongly, these changes cannot be assigned unambiguously to a specific base or molecular vibration.

Pronounced irradiation-associated changes were also observed at lower wavenumbers within the nucleobase region, where C=N and C=C stretching together with other coupled base vibrations contribute substantially to the spectral profile. In particular, features near 1546, 1462 and 1393 cm^{-1} were consistently highlighted by the average spectra (Fig. 2), difference spectra (Fig. 3), and PCA loading profile (Fig. 5). The change near 1462 cm^{-1} is particularly evident in the average spectra (Fig. 2), where irradiation is accompanied by the development of a distinct band, while near 1393 cm^{-1} a shoulder present in the non-irradiated spectrum develops into a more clearly resolved band. Taken together, the changes observed across the carbonyl- and C=N/C=C-dominated regions indicate that γ irradiation perturbs several components of the nucleobase vibrational environment rather than affecting a single isolated mode.

Previous vibrational spectroscopic studies have likewise identified nucleobase-associated modes as sensitive to ionizing radiation. Using FT-Raman spectroscopy, Sailer et al. reported dose-dependent changes in marker bands of all four nucleobases in γ irradiated DNA, together with base unstacking, modifications of the deoxyribose-phosphodiester framework and disruption of the B-form backbone[21]. However, these experiments studied substantially higher doses than those investigated here, reaching the kilogray range. Synytsya et al. subsequently examined calf-thymus DNA exposed to proton and γ irradiation at 0.5, 5 and 50 Gy using Raman spectroscopy[23]. Although nucleobase bands, particularly those associated with pyrimidines, were among the most radiation-sensitive spectral features, pronounced macromolecular damage was reported mainly at the highest investigated dose of 50 Gy.

Particularly relevant to the present work is the study undertaken by Shaw and Jirasek who investigated both calf-thymus DNA and short-stranded DNA using UV resonance Raman spectroscopy following irradiation with a medical Co^{60} source[24]. Their approach selectively enhanced nucleobase vibrations in the 1300-1700 cm^{-1} region and revealed radiation-induced disruption of base stacking and Watson–Crick hydrogen bonding in calf-thymus DNA. In the short-stranded DNA, however, base unstacking was less evident and the spectral response differed from that of the longer DNA system. Their experiments also covered doses extending to approximately 2000 Gy, well above the 0.3-100 Gy range examined in the present study. By contrast, Inman et al. demonstrated FTIR-based detection of X-ray exposure down to 0.1 Gy[30], but in a complex in vivo biological system rather than in a chemically defined DNA model.

To investigate the Mg^{2+}-dependent modulation of the radiation response, we examined the influence of the Mg/P ratio on the vibrational fingerprint and the results of the multivariate analysis. Although the same broad molecular regions remain involved across all Mg/P ratios, including nucleobase, sugar-phosphate and conformation-sensitive vibrations, their relative contributions and the corresponding dose-score trajectories depend strongly on the Mg/P ratio. Consequently, our results indicate that the Mg^{2+} ion atmosphere modulates the way in which the irradiation response is structurally expressed, which is particularly evident in the phosphate region. For the highest Mg^{2+} concentration, the contribution of the asymmetric PO_2^- stretching region to the irradiation-associated PC1 separation is relatively small, whereas stronger contributions are observed around the symmetric phosphate and neighbouring C-O/phosphodiester region (indicated by the corresponding positive loading near 1099 cm^{-1} in Fig. 5a). Conversely, for the lowest Mg concentration, a substantial positive irradiation-associated PC3 loading appears near 1203 cm^{-1}, in close proximity to the asymmetric PO_2^- vibration, together with a pronounced contribution near 1060 cm^{-1}. Taken together, decreasing Mg^{2+} content changes the relative involvement of phosphate-associated modes in the irradiation response.

A similar Mg^{2+} dependence is observed in the conformation-sensitive region below 900 cm^{-1}. Although the absolute sign of a PCA component is arbitrary, the relative direction of individual loading features becomes interpretable once the component orientation is referenced to the corresponding score distribution. As shown in Fig. 4a and Fig. 4c, the control groups (0 Gy) occupy the negative score direction for $r = 1$ and $r = 0.01$, whereas the irradiated samples are shifted toward more positive scores. Within this orientation, at $r = 1$, the feature near 872 cm^{-1} is associated predominantly with the control-related side of PC1, whereas positive features near 844 and 807 cm^{-1} contribute toward the irradiated samples (Fig. 5a). By contrast, at the lowest Mg/P ratio ($r = 0.01$), the feature near 868 cm^{-1}, associated with the A-form of DNA, becomes one of the most prominent positive contributions in the entire PC3 loading profile and the strongest positive feature within the conformation-sensitive region (Fig. 5b). Additional positive contributions are observed near 825 cm^{-1} and in the region around 800 cm^{-1}, which also contains conformation-sensitive, A-form-associated vibrations. Together, these features contribute toward the positive, irradiation-associated direction of the PC3 space, whereas neighbouring features around 848-843 cm^{-1} remain associated with the control-related direction. This redistribution of conformation-sensitive modes indicates that the conformational component of the irradiation-associated spectral response depends on the surrounding Mg^{2+} atmosphere. These changes in the conformation-sensitive bands suggest that the structural response of DNA to irradiation depends on the surrounding Mg^{2+} environment.

The dose-dependent PCA score trends further reinforce the previous findings. At $r = 1$, the mean PC1 scores of the 0.3-10 Gy groups remain comparatively close, followed by a pronounced displacement toward positive values at 30 and 100 Gy. This pattern is consistent with a comparatively buffered structural response over the lower absorbed-dose range. At $r = 0.1$, a substantial displacement is already evident at 10 Gy, with the trajectory reaching its highest PC2 value at 30 Gy before decreasing at 100 Gy. In the case of the lowest Mg^{2+} concentration, $r = 0.01$, even the lowest investigated absorbed dose of 0.3 Gy resulted in a pronounced shift from the strongly negative PC3 score of the control group toward the higher values representing the irradiation-associated samples. At higher absorbed doses, the distinction from the control group remained evident, but differences between the irradiated groups became less pronounced.

These distinct trends can be considered in the context of the polyelectrolyte nature of DNA. The negatively charged phosphate backbone creates a strong counterion atmosphere, while the presence of the positive Mg^{2+} atmosphere efficiently reduces the effective backbone charge through electrostatic screening and counterion condensation. Within the Manning framework, divalent cations provide more efficient charge compensation than monovalent ions, while in a mixed Na^+/Mg^{2+} atmosphere increasing the Mg^{2+} concentration shifts the counterion population toward a greater contribution of Mg^{2+} and a reduced contribution of Na^+ ions[10,14,15]. Our previous FTIR studies further showed that Mg^{2+}-DNA interactions are predominantly nonspecific and electrostatic, altering the phosphate environment and

hydration, and promoting stabilization of the DNA backbone rather than fixed site-specific binding[7]. Therefore, in the case of r = 1, the ion atmosphere represents a state of substantially greater electrostatic screening and charge-compensation than at r = 0.01. Previous measurements on short-chain DNA also showed that increasing r toward the value of 1 stabilizes the B-form and reduces the sensitivity of phosphate vibrations and overall conformation to changes in DNA concentration[18].

Within this framework, the relatively small differences in PC1 scores (r = 1) for doses between 0.3 and 10 Gy, are consistent with the relatively weak contribution of the asymmetric PO_2^- region to absorbed dose separation. This is in agreement with the DNA backbone whose electrostatic environment is more effectively screened and stabilized by the Mg^{2+} ion atmosphere. A substantially larger absorbed dose is then required before the irradiation-associated spectral fingerprint undergoes the pronounced multivariate displacement observed at 30-100 Gy. By contrast, at low Mg^{2+} content the phosphate charge is less effectively screened and the DNA helix is less constrained by divalent counterions. Irradiation-induced perturbations can therefore be expressed through phosphate and conformation-sensitive modes present even for the lowest absorbed dose, which is consistent with the pronounced shift in the PC scores from low control values. This indicates that even the lowest investigated dose of 0.3 Gy produces a marked response.

Taken together, the above observations imply a stabilizing and potentially protective role of Mg^{2+} against irradiation-induced structural perturbation. At higher Mg^{2+} content, stronger electrostatic screening and charge compensation appear to buffer the DNA backbone and delay the pronounced multivariate displacement to higher absorbed doses. However, since PCA scores and FTIR band changes do not directly quantify strand breaks or chemical lesion yield, the present data cannot establish radioprotection in a strict damage-yield sense. Rather, they indicate that Mg^{2+} attenuates and redistributes the structural manifestation of the irradiation response across the DNA vibrational fingerprint. Therefore, Mg^{2+} appears not only to modulate the radiation response, but also to confer a degree of structural protection by changing the pathway through which irradiation-induced perturbations are expressed.

Beyond the clear separation between non-irradiated and irradiated DNA, the PCA score trends also contain information related to absorbed dose. For each Mg/P ratio, the mean score of the principal component carrying the irradiation-associated variance changed across the investigated dose range (Fig. 6), although the degree of separation between individual dose groups depended strongly on the Mg^{2+} environment. At r = 1 the highest absorbed doses, 30 and 100 Gy, were clearly separated from the lower-dose groups, whereas at r = 0.1, the 10 Gy group was distinctly resolved from the lowest doses. These differences indicate that dose-associated information is encoded in the multivariate spectral response and that its expression depends on the Mg^{2+} environment.

Together with the corresponding loading profiles, these score distributions show that γ irradiation produces not only detectable changes in the DNA vibrational fingerprint, but also a structured spectral response that retains information related to absorbed dose. This provides a proof of concept that FTIR combined with multivariate analysis can detect radiation exposure and reveal spectroscopic information related to absorbed dose in a controlled DNA-Mg^{2+} system. These findings support the further development of this approach toward molecular radiation sensing and quantitative absorbed-dose estimation.

The present PCA analysis is descriptive and unsupervised, and should therefore not be interpreted as quantitative dose prediction. Our future work will focus on identifying the spectral regions most informative for dose discrimination and on evaluating their potential for quantitative absorbed-dose estimation. Although predictive modelling and validation represent important next steps, they are beyond the scope of the present study.

5. Conclusions

Gamma irradiation produces systematic changes in the FTIR fingerprint of ultra-short DNA across nucleobase, sugar-phosphate and conformation-sensitive spectral regions, with detectable differences

already at 0.3 Gy. Principal component analysis clearly separated non-irradiated from irradiated samples and revealed dose-associated spectral organization. Importantly, the form of this response depended on the Mg^{2+} ion atmosphere, indicating that Mg^{2+} modulates the structural pathway through which irradiation-induced perturbations are expressed. The observed spectral patterns indicate a stabilizing influence, and potentially protective role of Mg^{2+} on DNA under irradiation.

Additionally, the observed results demonstrate that FTIR spectroscopy combined with multivariate analysis can detect γ radiation-induced molecular changes in a controlled DNA-Mg^{2+} system, and the resulting spectral fingerprint retains information related to absorbed dose. Importantly, understanding the interplay between absorbed dose and local chemical environment provides a foundation for translating this approach from controlled DNA models toward more complex biological systems. This provides a proof of concept for FTIR-based molecular radiation sensing. Our future work will focus on utilizing the identified dose-informative spectral regions to refine the spectroscopic protocol and optimize quantitative absorbed-dose estimation through predictive modeling and validation.

Funding

This research was funded by the European Union - NextGenerationEU under the project *Biological Effects of Ionizing Radiation: Insights from Vibrational Spectroscopy*, grant number 10106-25-2999.

Acknowledgements

The authors gratefully acknowledge Josip Basić, Martin Bobek, Antonia Lovrenčić, Lucija Totić, and Nikola Šegedin for their assistance with sample preparation and experimental measurements.

Data Availability

The datasets generated and analysed during the current study are available from the corresponding author upon reasonable request.

Additional Information

The authors declare no competing interests.

References

[1] Russ, E., Davis, C. M., Slaven, J. E. & Bradfield, D. T. Comparison of the medical uses and cellular effects of high and low linear energy transfer radiation. Toxics 10, 628 (2022).

[2] Melia, E. & Parsons, J. L. DNA damage and repair dependencies of ionising radiation modalities. Bioscience Reports 43, BSR20222586 (2023).

[3] Radstake, W. E., Parisi, A., Denbeigh, J. M., Furutani, K. M. & Beltran, C. J. DNA double-strand break repair kinetics after exposure to photons and ions: A systematic review. Radiation Research 201, 604–616 (2024).

[4] Zhang, C., Liu, J., Wu, J., Ranjan, K., Cui, X., Wang, X., Zhang, D. & Zhu, S. Key molecular DNA damage responses of human cells to radiation. Frontiers in Cell and Developmental Biology 12, 1422520 (2024).

[5] Schlathölter, T. & Poully, J.-C. Radiation-induced molecular processes in DNA: A perspective on gas-phase interaction studies. Chemistry – A European Journal 30, e202400633 (2024).

[6] KC, S. & Abolfath, R. Towards the ionizing radiation induced bond dissociation mechanism in oxygen, water, guanine and DNA fragmentation: a density functional theory simulation. Scientific Reports 12, 19853 (2022).

[7] Park, J., Jung, K.-W., Kim, M. K., Gwon, H.-J. & Jung, J.-H. New damage model for simulating radiation-induced direct damage to biomolecular systems and experimental validation using pBR322 plasmid. Scientific Reports 12, 11345 (2022).

[8] Beaudier, P., Zein, S. A., Chatzipapas, K., Tran, H. N., Devès, G., Plawinski, L., Liénard, R., Dupuy, D., Barberet, P., Incerti, S., Gobet, F. & Seznec, H. Quantitative analysis of dose dependent DNA fragmentation in dry pBR322 plasmid using long read sequencing and Monte Carlo simulations. Scientific Reports 14, 18650 (2024).

[9] Bloomfield, V. A., Crothers, D. M. & Tinoco, I. Physical Chemistry of Nucleic Acids. 400–465 (Harper & Row, 1974).

[10] Manning, G. S. Molecular theory of polyelectrolyte solutions with applications to electrostatic properties of polynucleotides. Q. Rev. Biophys. 11, 179–246 (1978).

[11] Dobrynin, A. V. & Rubinstein, M. Theory of polyelectrolytes in solutions and at surfaces. Prog. Polym. Sci. 30, 1049–1118 (2005).

[12] Cherstvy, A. G. Electrostatic interactions in biological DNA-related systems. Phys. Chem. Chem. Phys. 13, 9942–9968 (2011).

[13] Pevsner, A. & Diem, M. Infrared spectroscopic studies of major cellular components. Part II: The effect of hydration on nucleic acids. Biopolymers 62, 282–293 (2001).

[14] Serec, K., Dolanski Babić, S., Podgornik, R. & Tomić, S. Effect of magnesium ions on the structure of DNA thin films: an infrared spectroscopy study. Nucleic Acids Res. 44, 8456–8464 (2016).

[15] Serec, K., Dolanski Babić, S. & Tomić, S. Magnesium ions reversibly bind to DNA double stranded helix in thin films. Spectrochim. Acta A Mol. Biomol. Spectrosc. 268, 120663 (2022).

[16] Tomić, S. et al. Short-fragment Na-DNA dilute aqueous solutions: fundamental length scales and screening. Europhys. Lett. 81, 68003 (2008).

[17] Waters, J. T. et al. Transitions of double-stranded DNA between the A- and B-forms. J. Phys. Chem. B 120, 8449–8456 (2016).

[18] Serec, K. et al. Ultra-short DNA fragments undergo A-to-B conformational transitions revealed by FTIR spectroscopy. Int. J. Mol. Sci. 27, 1876 (2026).

[19] Schröter, M.-A., Meyer, S., Hahn, M. B., Solomun, T., Sturm, H. & Kunte, H. J. Ectoine protects DNA from damage by ionizing radiation. Scientific Reports 7, 15272 (2017).

[20] Anastassopoulou, J. & Theophanides, T. Magnesium–DNA interactions and the possible relation of magnesium to carcinogenesis: irradiation and free radicals. Crit. Rev. Oncol. Hematol. 42, 79–91 (2002).

[21] Sailer, K., Viaggi, S. & Nüsse, M. Radiation-induced structural modifications in dsDNA analysed by FT-Raman spectroscopy. Int. J. Radiat. Biol. 69, 601–613 (1996).

[22] Gault, N. & Lefaix, J.-L. Infrared microspectroscopic characteristics of radiation-induced apoptosis in human lymphocytes. Radiat. Res. 160, 238–250 (2003).

[23] Synytsya, A. et al. Raman spectroscopic study of calf thymus DNA: an effect of proton- and γ-irradiation. J. Raman Spectrosc. 38, 1406–1415 (2007).

[24] Shaw, C. P. & Jirasek, A. The use of ultraviolet resonance Raman spectroscopy in the analysis of ionizing-radiation-induced damage in DNA. Appl. Spectrosc. 63, 412–422 (2009).

[25] Meade, A. D., Clarke, C., Byrne, H. J. & Lyng, F. M. Fourier transform infrared microspectroscopy and multivariate methods for radiobiological dosimetry. Radiat. Res. 173, 225–237 (2010).

[26] Maguire, A. et al. Analyses of ionizing radiation effects in vitro in peripheral blood lymphocytes with Raman spectroscopy. Radiat. Res. 183, 407–416 (2015).

[27] Lasalvia, M. et al. Raman spectroscopy for the evaluation of the radiobiological sensitivity of normal human breast cells at different time points after irradiation by a clinical proton beam. Analyst 144, 2097–2108 (2019).

[28] Ricciardi, V., Portaccio, M., Manti, L. & Lepore, M. An FTIR microspectroscopy ratiometric approach for monitoring X-ray irradiation effects on SH-SY5Y human neuroblastoma cells. Appl. Sci. 10, 2974 (2020).

[29] Ciobanu, C. et al. Exploring the use of Raman spectroscopy and covariate-adjusted multivariate analysis for the detection of irradiated blood. Radiat. Res. 199, 396–405 (2023).

[30] Inman, J. L. et al. Long-term, non-invasive FTIR detection of low-dose ionizing radiation exposure. Sci. Rep. 14, 6119 (2024).

[31] Martínez-Rovira, I. et al. Infrared microspectroscopy to elucidate the underlying biomolecular mechanisms of FLASH radiotherapy. Radiother. Oncol. 196, 110238 (2024).

[32] Wanstall, H. C. et al. VHEE FLASH sparing effect measured at CLEAR, CERN with DNA damage of pBR322 plasmid as a biological endpoint. Sci. Rep. 14, 14803 (2024).

[33] Heck, B., Jess-Hempen, A., Kreiner, H. J., Schöpgens, H. & Mack, A. Accuracy and stability of positioning in radiosurgery: Long term results of the Gamma Knife system. Medical Physics 34, 1487–1495 (2007).

[34] Serec, K., Šegedin, N., Krajačić, M. & Dolanski Babić, S. Conformational transitions of double-stranded DNA in thin films. Applied Sciences 11, 2360 (2021).

[35] Zhang, Z.-M., Chen, S. & Liang, Y.-Z. Baseline correction using adaptive iteratively reweighted penalized least squares. Analyst 135, 1138–1146 (2010).

[36] Barnes, R. J., Dhanoa, M. S. & Lister, S. J. Standard normal variate transformation and de-trending of near-infrared diffuse reflectance spectra. Appl. Spectrosc. 43, 772–777 (1989).

[37] Martens, H., Høy, M., Wise, B. M., Bro, R. & Brockhoff, P. B. Pre-whitening of data by covariance-weighted pre-processing. J. Chemom. 17, 153–165 (2003).

[38] Wood, B. R. The importance of hydration and DNA conformation in interpreting infrared spectra of cells and tissues. Chemical Society Reviews 45, 1980–1998 (2016).

[39] Letellier, R., Ghomi, M. & Taillandier, E. Interpretation of DNA vibration modes: IV—A single-helical approach to assign the phosphate-backbone contribution to the vibrational spectra in A and B conformations. Journal of Biomolecular Structure and Dynamics 6, 755–768 (1989).

[40] Abdi, H. & Williams, L. J. Principal component analysis. Wiley Interdisciplinary Reviews: Computational Statistics 2, 433–459 (2010).

[41] Lipiec, E. et al. A new approach to studying the effects of ionising radiation on single cells using FTIR synchrotron microspectroscopy. Radiat. Phys. Chem. 93, 135–141 (2013).

[42] Lipiec, E., Sekine, R., Bielecki, J., Kwiatek, W. M. & Wood, B. R. Molecular characterization of DNA double-strand breaks with tip-enhanced Raman scattering. Angew. Chem. Int. Ed. 53, 169–172 (2014).

LIST OF FIGURES

Figure 1. In-house developed sample holder and irradiation geometry used for γ irradiation of DNA solutions. (a) Custom-made sample holders designed for positioning the DNA solution samples during irradiation. (b) Sample holder positioned within the spherical irradiation PMMA phantom. (c) Schematic representation of the Gamma Knife irradiation geometry, illustrating the convergence of Co-60 γ-ray beams toward the DNA sample positioned at the irradiation isocentre. (d) Sagittal CT image of the phantom and insert in the Leksell GammaPlan treatment planning system, showing the planned 10 Gy absorbed-dose distribution at the sample position; the dose distribution is indicated by the yellow contour and the insert/sample position by the red reference lines.

Figure 2. Average FTIR spectra of non-irradiated (0 Gy) and irradiated short-chain DNA thin films in the 1800–700 cm^{-1} spectral range for r = 1, 0.1 and 0.01 are presented in panels (a) to (c), respectively, with irradiated samples exposed to Co-60 γ rays at absorbed doses of 0.3, 1, 10, 30 and 100 Gy. Selected band positions exhibiting irradiation-associated spectral changes are indicated.

Figure 3. FTIR difference spectra of short-chain DNA thin films irradiated with Co-60 γ- rays at absorbed doses of 0.3, 1, 10, 30 and 100 Gy for three magnesium-to-phosphate molar ratios: (a) r = 1, (b) r = 0.1, and (c) r = 0.01. Difference spectra were calculated for each Mg/P condition as $\Delta A = A_{dose} - A_{control}$, where the corresponding non-irradiated sample (0 Gy) served as the control. Irradiation-associated spectral changes are observed throughout the nucleobase region (1800–1300 cm^{-1}), the sugar–phosphate backbone region (1300–900 cm^{-1}), and the conformation-sensitive region below 900 cm^{-1}. Difference spectra were vertically offset for clarity.

Figure 4. Principal component analysis (PCA) score plots of FTIR spectra from non-irradiated and γ irradiated short-chain DNA samples for three magnesium-to-phosphate molar ratios: (a) r = 1, (b) r = 0.1, and (c) r = 0.01. Samples correspond to absorbed doses of 0, 0.3, 1, 10, 30 and 100 Gy. The variance explained by each principal component is indicated on the respective axes. Non-irradiated controls occupy a distinct region of the PCA score space relative to irradiated samples, while additional dose-associated organization is observed within the irradiated groups.

Figure 5. PCA loading profiles highlighting the spectral regions contributing to irradiation-associated separation of short-chain DNA samples at different magnesium-to-phosphate molar ratios. (a) PC1 loading profile for r = 1, (b) PC3 loading profile for r = 0.01. Major loading features are observed in the nucleobase, sugar–phosphate backbone and conformation-sensitive regions.

Figure 6. Dose-dependent PCA scores for the principal component along which the clearest separation between non-irradiated and irradiated samples was observed at each magnesium-to-phosphate molar ratio: (a) PC1 for r = 1, (b) PC2 for r = 0.1, and (c) PC3 for r = 0.01. Individual scores are presented together with the mean values and the corresponding standard deviations for each absorbed dose. The results show systematic

dose-associated changes in the FTIR spectral fingerprint, with the response pattern depending on the Mg/P ratio.

LIST OF TABLES

Table 1. Absorbed dose values delivered to the DNA solution samples, with associated uncertainties and corresponding irradiation times.
Table 2. Principal FTIR absorption bands identified in the non-irradiated (0 Gy) short-chain DNA thin film spectra in the 1800-700 cm^{-1} fingerprint region and their tentative literature/based vibrational assignments[13,14,17,18,34,38,39].

AUTHOR CONTRIBUTIONS

K.S. and S.D.B. developed the study concept and contributed to the study design. K.S., S.D.B. and H.H. contributed to the development of the experimental methodology. K.S. carried out the experimental work, coordinated the research activities and was responsible for project administration. H.H. was responsible for the irradiation experiments, including irradiation procedures, dose control and radiation safety. M.K. implemented and validated the Python-based data analysis workflow. K.S. and M.K. performed the data processing, formal analysis and interpretation of the results and were responsible for data curation. K.S., M.K. and H.H. contributed to data visualization and preparation of the figures. H.H., K.S. and O.G. provided the resources required for the study. K.S. prepared the original draft of the manuscript, taking the lead in manuscript preparation. K.S., M.K., H.H. and S.D.B. critically reviewed and edited the manuscript. All authors have read and approved the final version of the manuscript.